

Entanglement spectrum of the two dimensional Bose-Hubbard model

Vincenzo Alba,¹ Masudul Haque,² and Andreas M. Läuchli³

¹*Department of Physics and Arnold Sommerfeld Center for Theoretical Physics,
Ludwig-Maximilians-Universität München, D-80333 München, Germany*

²*Max-Planck-Institut für Physik komplexer Systeme, Nöthnitzer Straße 38, D-01187 Dresden, Germany*

³*Institut für Theoretische Physik, Universität Innsbruck, A-6020 Innsbruck, Austria*

(Dated: January 9, 2013)

We study the entanglement spectrum (ES) of the Bose-Hubbard model on the two dimensional square lattice at unit filling, both in the Mott insulating and in the superfluid phase. In the Mott phase, we demonstrate that the ES is dominated by the physics at the boundary between the two subsystems. On top of the boundary-local (perturbative) structure, the ES exhibits substructures arising from one-dimensional dispersions along the boundary. In the superfluid phase, the structure of the ES is qualitatively different, and reflects the spontaneously broken $U(1)$ symmetry of the phase. We attribute the basic low-lying structure to a so-called “tower of states” (TOS) Hamiltonian of the model. We then discuss how these characteristic structures evolve across the superfluid to Mott insulator transition and their influence on the behavior of the entanglement entropies. Finally, we briefly outline the implications of the ES structure on the efficiency of matrix-product-state based algorithms in two dimensions.

Introduction — In recent years the cross fertilization between quantum information and condensed matter has led to new insights into the physics of low dimensional systems [1]. In particular the concept of *entanglement spectrum* has established itself as an informative and intriguing theme. Considering a bipartition of a system into parts A and B , the entanglement spectrum (ES), $\{\xi_i\}$, is defined in terms of the Schmidt decomposition

$$|\psi\rangle = \sum_i e^{-\xi_i/2} |\psi_i^A\rangle \otimes |\psi_i^B\rangle. \quad (1)$$

Here $|\psi\rangle$ is the ground state, and the states $|\psi_i^A\rangle$ ($|\psi_i^B\rangle$) form an orthonormal basis for subsystem A (B). The ES $\{\xi_i = -\log \lambda_i\}$ can also be thought of as the spectrum of the so called entanglement hamiltonian $\mathcal{H}_E \equiv -\log \rho_A$ where the reduced density matrix ρ_A is obtained after tracing out the B part of the system density matrix $|\psi\rangle\langle\psi|$. The ES can also be used to construct *entanglement entropies* (Renyi and von Neumann) which quantify the entanglement between the two subsystems.

Many results are now available for the ES and entanglement entropies of one-dimensional (1D) systems. In contrast, higher dimensions are far less explored. Much of the ES literature on 2D systems focuses on topological phases [2]. A detailed understanding of generic ES features for more common 2D systems is not currently available.

In this work we present a thorough investigation of the ES for the 2D Bose-Hubbard model [3, 4]. We extract features for both the gapped Mott insulator and the superfluid (gapless, symmetry-broken) phases. This analysis provides insights into the ES which, in addition to the intrinsic importance of the Bose-Hubbard model, are likely to be generic to gapped and symmetry-broken gapless 2D phases. Our analysis is based on DMRG calculations on a cylindrical geometry, complemented by perturbative calculations (Mott phase) and by analysis of the tower of states analogy (superfluid phase).

In the Mott insulator, the ES is “boundary-local” in the

sense introduced in Ref. [5] for 1D gapped systems. In 1D gapped phases adiabatically connected to a “simple” state (product state or low-entanglement state), the ES is organized in a perturbative or hierarchical structure closely linked to boundary-locality: higher levels in the ES corresponding to excitations farther from the boundary [5]. The present work shows how ES features of the 2D Mott insulator can be understood from this viewpoint. In 2D the boundary is an extended object and not a single point. In the ES, this shows up as a multiplicity structure superposed on top of the perturbative one: there are multiple ES states for each order of the perturbative hierarchy. This reflects the physics that excitations created close to the boundary can move without changing the distance from the boundary, resulting in dispersion structures within the ES at every order. This can be cast in the language of entanglement Hamiltonians (\mathcal{H}_E) for which we provide some analytic perturbative expressions. We also provide analytic perturbative expressions for several entanglement entropies (von Neumann and Renyi) in the gapped phase, and discuss how area laws emerge in the perturbative framework. We believe that these features of the ES in the Mott phase (boundary-locality, multiplet structure, 1D dispersions, etc) are general for (non-topological) 2D gapped systems (gapped fermionic models, Heisenberg XXZ, etc.).

At the transition between the Mott and superfluid phases the ES structure changes dramatically. We show that its lower part (which we call ES “envelope”) sharply reflects the different nature of the two phases.

An intriguing feature of the ES in phases with a broken continuous symmetry is the relation [6] between its lower part and the so-called tower of states (TOS) *energy* spectrum obtained when a system with continuous symmetry breaking in the thermodynamic limit is placed in a finite volume [7]. We demonstrate that in the superfluid phase the ES envelope, separated from the rest of the spectrum by an apparent “entanglement gap”, reflects the appropriate TOS Hamiltonian. This correspondence provides a framework to understand generic

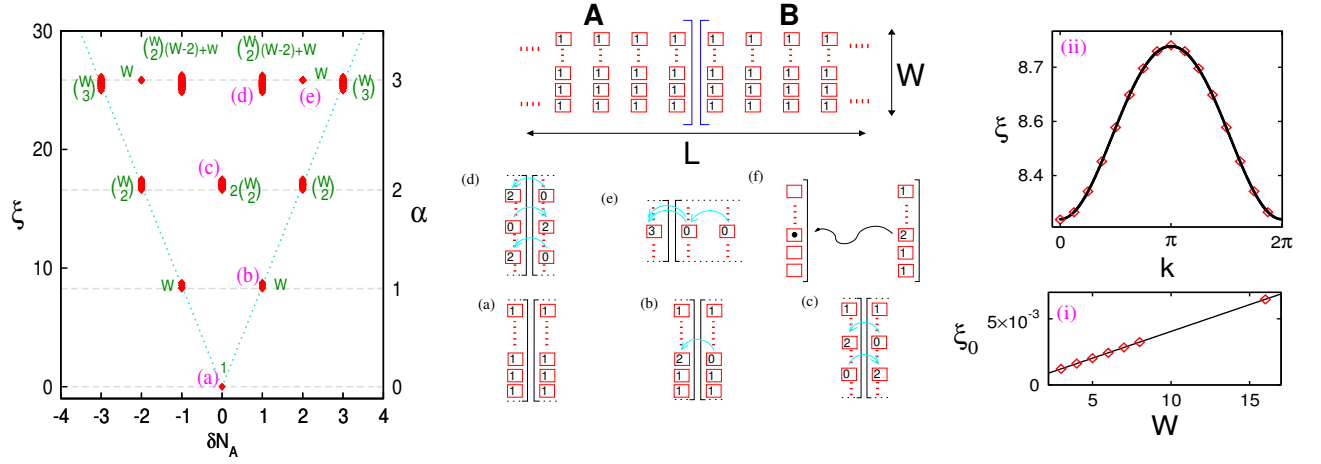


FIG. 1: ES in the Mott phase. **(left)** Perturbative structure, DMRG data for equally bipartitioned cylinder, $W = 8, L = 32, U = 100$. Multiplicities are indicated near each group of states. The dotted lines highlight the ES envelope. **(center bottom)** Bosonic configurations corresponding to leading order configurations for some ES levels. Only occupancies on sites nearer the boundary are shown (omitted sites are singly occupied). We restrict to $\delta N_A \geq 0$. The arrows represent hopping (perturbative) processes to create a given configuration. In (f) we show the effective single particle (boundary) excitation corresponding to multiplet (b). **(right)** Entanglement dispersions. Data points are DMRG ($U = 100$); black lines are perturbative results. **(i)** Lowest ES level ξ_0 as a function of W . **(ii)** Entanglement dispersion for the lowest ES multiplet at $\delta N_A = 1$. k denotes the momentum along the boundary.

features of the ES envelope.

The Bose-Hubbard model — We consider the two dimensional Bose-Hubbard model on a cylinder of length L (with open boundary conditions) and circumference W (with periodic boundary conditions). The Hamiltonian is $\mathcal{H} = -\sum_{\langle ij \rangle} (b_i^\dagger b_j + h.c.) + \frac{U}{2} \sum_i n_i(n_i - 1)$ where b_i are bosonic operators, $n_i = b_i^\dagger b_i$, and U is the on-site repulsion. We restrict to the case of unit filling. To calculate the ES we divide the cylinder in two parts A and B of size V_A and V_B respectively, with W the boundary length (Fig. 1 center top). The number of bosons $N_A(N_B)$ in $A(B)$ is a good quantum number for the ES and can be used to label the ES levels. It is convenient to introduce $\delta N_A \equiv N_A - V_A$ measuring the excess of bosons in A with respect to unit filling. Since the system has translational invariance along the boundary, the corresponding momentum k is a good quantum number.

The ES in the Mott insulator — In the $U \rightarrow \infty$ limit, the ground state is a product state with one boson per site. The ES has only one level, $\xi_0 = 0$. As in Ref. [5], the ES at large U can be constructed through boundary-linked perturbation theory, treating the hopping term $\mathcal{H}_p \equiv -\sum_{\langle ij \rangle} (b_i^\dagger b_j + h.c.)$ as perturbation.

Fig. 1 (left) plots the ES $\{\xi\}$ for a system at $U = 100$ (DMRG data). We denote with α the perturbative order giving the leading contribution to the ES levels. As in gapped 1D systems [5], the separation ($\sim \log U$) between consecutive α reflects the perturbative nature of the ES. In the center bottom we show the configurations giving dominant contribution to selected groups of ES levels. The A part of these configurations also gives the dominant configuration in the entanglement eigenfunctions (eigenfunctions of ρ_A). At each δN_A and $\alpha > 0$ there is more than one level. The multiplicities are

determined by the boundary length W , and can be understood in terms of hopping processes across the boundary. On the ES envelope (dotted line in Fig. 1 left), the group of levels at δN_A is obtained by transferring δN_A bosons from subsystem B to A . This process appears at order δN_A (with amplitude $U^{-\delta N_A}$). The multiplicity $m(\delta N_A)$ is obtained as the number of ways of moving δN_A bosons across the boundary to give distinct configurations, i.e. $m(\delta N_A) = C(W, \delta N_A)$ with C the binomial coefficient (see (a)(b) in Fig. 1 center).

Similar boundary perturbative processes help explain ES levels above the envelope; c.f., (c)(d)(e) in Fig. 1 left and center. At $\alpha < 3$ the leading order of all ES levels (not only the envelope) is given by pure boundary processes. At higher orders ($\alpha \geq 3$) processes further away from the boundary start contributing to the leading order of some ES levels, e.g., (e) in Fig. 1. The corresponding configurations involve hoppings perpendicular to the boundary, and thus are similar to the physics of ES configurations in 1D chains [5]. This is reflected in the linear multiplicity ($\sim W$) in (e). Generically, the multiplicities grow exponentially with α ($\sim W^\alpha$). This growth of multiplicity is related to the area law of entanglement entropy which limits the performance of DMRG in 2D systems even in gapped phases.

Entanglement dispersions & entanglement Hamiltonian —

We now examine the substructures superposed on the perturbative hierarchy of ES levels. As the simplest example, we consider the lowest ES states at $\delta N_A = 1$, marked (b) in Fig. 1. These W states are composed from particle-hole excitations across the boundary at the W possible positions along the boundary. Fig 1(f) shows how this local excess/depletion of bosons can be regarded as a boundary degree of freedom. Since the momentum k along the boundary is a good quan-

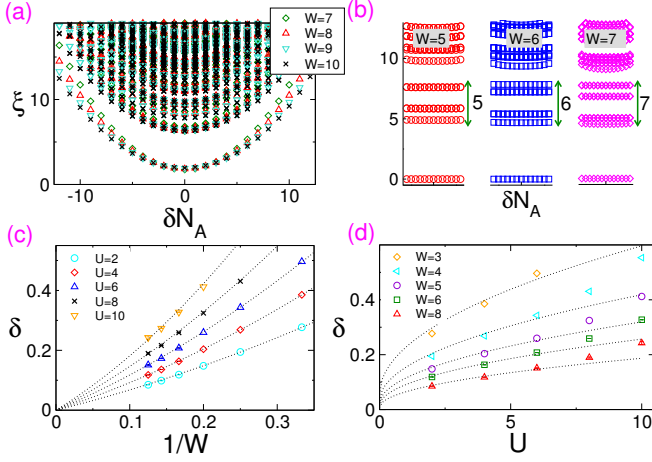


FIG. 2: (a) ES in the superfluid phase (DMRG data at $U = 2$ for size $L/4 = W$). (b) The same ES as in (a) but after subtracting the contribution of the envelope. (c) Spacing δ (defined in text and Fig. 3) plotted versus $1/W$; various U . Dotted lines are fits to $A/W + B/W^2$. (d) δ as function of U . Dotted lines are fits to $\delta \sim \sqrt{U}$ (expected for $U \rightarrow 0$).

tum number, in the entanglement eigenstates these excitations will not be localized, but will appear as momentum eigenstates, similar to a single-particle dispersion. This “entanglement dispersion” is given perturbatively up to $\mathcal{O}(U^{-3})$ as

$$\xi_k = \log(U^2/2) + 2(2W + 10)/U^2 - 24 \left[1/U + (2W - 25)/U^3 \right] \cos k - 68/U^2 \cos 2k + 552/U^3 \cos 3k. \quad (2)$$

Comparison with DMRG data ($U = 100$, $W = 8$) is shown in Fig. 1 right panel (ii).

The spectrum (2) can be interpreted as the spectrum of the “Hamiltonian” $\mathcal{H}_E = \text{const.} + \sum_{i,r} A_r (a_i^\dagger a_{i+r} + h.c.)$ where i labels sites of the boundary and a_i are the boundary degrees of freedom. This entanglement Hamiltonian is a boundary Hamiltonian of single particle tight-binding form, with hopping amplitudes A_r decaying exponentially with distance r [8, 9]. These results can be generalized to each group of states on the ES envelope: the envelope states in sector δN_A are described by a boundary entanglement Hamiltonian \mathcal{H}_E for δN_A particles. Expressions for \mathcal{H}_E can be obtained perturbatively [9]. Up to lowest subleading order, \mathcal{H}_E is of nearest neighbor tight-binding form (on a chain).

As the Mott-superfluid transition is approached, \mathcal{H}_E becomes more and more long range [8, 9], similar to the correlation length which diverges upon approaching the phase transition.

The ES in the superfluid phase — In the superfluid phase ($U \lesssim 16.739$ [10]) the ES looks dramatically different (Fig. 2). There is a clearer separation between a low-lying “envelope” and the rest of the ES, but the envelope now has quadratic dependence on δN_A , and there is only a single envelope level at each δN_A . These features are due to the fact that the underlying superfluid state has spontaneous breaking

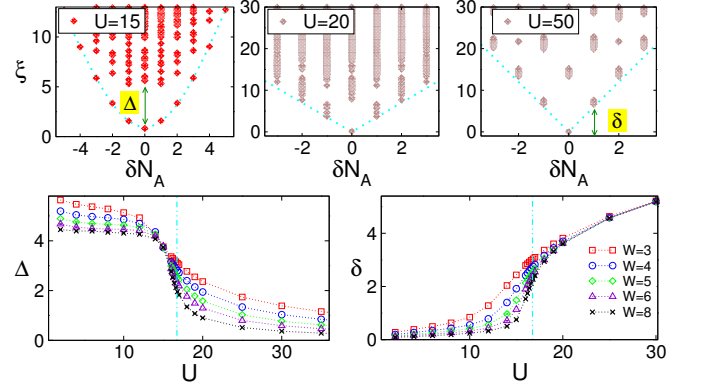


FIG. 3: (top) Restructuring of ES across the Mott-superfluid transition (DMRG data for $W = 8 = L/4$, equal bipartitions). The arrows explain the definitions of the quantities Δ and δ . (bottom) Δ and δ plotted versus U for several values of the boundary length W . The vertical line denotes the critical value U_c .

of $U(1)$ symmetry in the thermodynamic limit. We can explain some of these features through a correspondence with the tower of states spectrum [7], which is the physical low-energy spectrum obtained when a system with spontaneously broken continuous symmetry is placed in a finite volume. Since the finite-size ES is plotted against quantum numbers whose conservation is spontaneously broken only in the thermodynamic limit, it is naturally related to the TOS spectrum. The precise relation [6] is that for the lower part of the ES $\mathcal{H}_E \sim \mathcal{H}_T/T_E$ where \mathcal{H}_T is the TOS Hamiltonian, T_E is an effective temperature given by $T_E = v_s/\mathcal{L}$ with v_s the velocity of the gapless excitations (for the Bose Hubbard this is the sound velocity), and $\mathcal{L} \approx W$ is the linear size of the system. The form of T_E reflects the finite size behavior of the sound-wave gap. For the Bose-Hubbard the TOS Hamiltonian is $\mathcal{H}_T \sim (\delta \tilde{N})^2/(\chi V)$ where \tilde{N} is the total particle number operator and $\chi \equiv dn/d\mu$ is the compressibility. This suggests that $\mathcal{H}_E \sim \frac{W}{v_s \chi V_A} (\delta N_A)^2 \sim (\delta N_A)^2/(v_s \chi W)$.

We characterize this scenario through the quantities Δ (“TOS gap”) and δ (“envelope curvature”), defined pictorially in Fig. 3. Formally, $\delta \equiv \xi_{k=0} - \xi_0$ and $\Delta \equiv \xi_{k=2\pi/W} - \xi_{k=0}$, with $\xi_{k=0}, \xi_{k=2\pi/W}$ in the lowest ES multiplet at $\delta N_A = 1$, while ξ_0 is the lowest ES level. In the thermodynamic limit $\mathcal{H}_E \sim \mathcal{O}(1/W)$, then $\delta \sim \mathcal{O}(1/W)$. Furthermore, in the limit $U \rightarrow 0$ at fixed W , using $\chi^{-1} \sim U$ and $v_s \sim \sqrt{U}$ one obtains $\delta \sim \sqrt{U}$. Finally, assuming that the lowest excitations above the ES envelope are sound-wave like one can write $\mathcal{H}_E \sim [\mathcal{H}_T + \mathcal{H}_{sw}]/T_E$ where \mathcal{H}_{sw} describes the sound wave excitations. Since $T_E \sim 1/W$ this suggests that the gap Δ remains finite in the thermodynamic limit, although logarithmic decay cannot be ruled out [11].

Numerical data shown in Figs. 2 and 3 supports this picture. The presence of a finite gap Δ for all the values of W and the quadratic behavior of the ES envelope provide some confirmation of the tower of states picture. Figs. 2 (c) and 2 (d) show good agreement with the predictions $\delta \sim 1/W$ and $\delta \sim \sqrt{U}$.

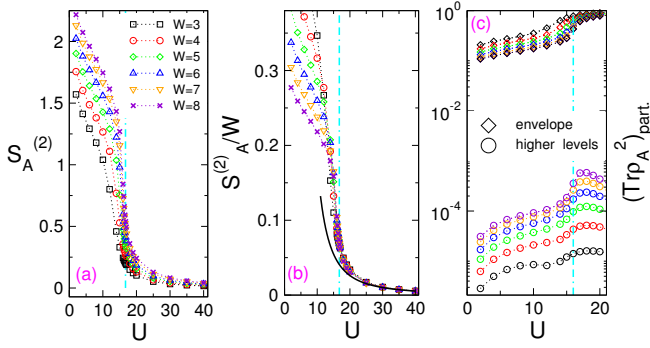


FIG. 4: **(a,b)** Renyi entropy $S_A^{(2)}$ (DMRG data). In **(b)** the data of **(a)** is rescaled by boundary length W , and the continuous line is the perturbative result. **(c)** Contributions to $\text{Tr} \rho_A^2$ from the envelope ES levels (rhombi) and from the higher levels (circles). Vertical lines in each panel marks the transition point.

In Fig. 2 (b) and 3 we notice also that the gap Δ hardly changes with W (although a $\sim 1/\log W$ type of decay cannot be ruled out with these sizes.) Surprisingly, Δ is also constant as a function of δN_A . We also note that, above the gap, the ES levels possess further band-like structures with a band of W levels of width comparable to Δ , slightly but distinctly separated from higher levels. Field theory arguments involving the dynamics of sound waves indicate similar structures [11].

At the $U = 0$ point, the ES can be calculated exactly [9, 12]. There is a single ES level for each δN_A , i.e., only the envelope survives and the rest of the ES is pushed to infinity. The wavefunction for $U = 0$ is an exact Bose condensate; the highly symmetric situation is similar to the ferromagnetic case [13].

The Mott-superfluid transition — Across the phase transition ($U_c \approx 16.739$ [10]), Δ and δ show “dual” behaviors (Fig. 3 bottom). In the Mott insulating phase, $\Delta \sim 1/W^2$ (from (2) one has $W^2 \Delta \sim \pi^2/6$), while in the superfluid Δ converges to a possibly nonzero value or vanishes only logarithmically with W [11]. In contrast, the W -dependence of δ is: $\delta \sim \text{const.}$ in the Mott insulator; $\delta \rightarrow 0$ in the superfluid. The observed finite size scaling behavior of δ suggests that this quantity might allow a scaling collapse, similar to the 1D example of Ref. [14]. For the 2D transverse field Ising model the closing of a quantity similar to δ at the quantum critical point has also been reported [15].

Entanglement entropies — In the Mott phase all the entropies can be constructed perturbatively in $1/U$. Perturbative considerations for entanglement entropies in 2D gapped phases also appear in Refs. [16–19]. We first consider the lowest ES level ξ_0 which is the single-copy entanglement, $\lim_{\gamma \rightarrow \infty} S_A^{(\gamma)}$ with $S^{(\gamma)} \equiv -\log \text{Tr} \rho_A^\gamma / (\gamma - 1)$ the Renyi entropy of index γ . Up to $\mathcal{O}(U^{-4})$ we find $\xi_0 = cW$ with $c = 4/U^2 + 488/U^4$, i.e. the expected area law behavior. Fig. 1(i) compares with DMRG data at $U = 100$. The dependence on W in perturbation theory is tricky [9]. Remarkably, up to $\alpha = 4$ the only dependence is the linear area law and higher powers in W disappear in the entropy. The same is true for

the von Neumann entropy,

$$S_A/W = \frac{4}{U^2} - \frac{4}{U^2} \log \frac{2}{U^2} - \frac{64}{U^4} \log \frac{2}{U^2} - \frac{584}{U^4} + \mathcal{O}(U^{-6}),$$

and the Renyi entropies with $\gamma = 2, 3$,

$$S_A^{(2)}/W \approx 8/U^2 + 968/U^4 \quad S_A^{(3)}/W \approx 6/U^2 + 1464/U^4.$$

In the superfluid ($0 \leq U < U_c$) the entropies are still expected to exhibit an area law, although, due to the symmetry breaking, subleading logarithmic corrections arise [6, 19, 20], i.e. $S_A^{(n)} \sim c_1 W + c_2 \log W$. Moreover, at $U = 0$ there is pure logarithmic behavior $S_A \sim 1/2 \log N_A$ [9]. This implies that the area law coefficient vanishes as $U \rightarrow 0$ and the entanglement entropies are dominated by the logarithmic corrections up to larger systems sizes as U decreases.

The transition between these different regimes is illustrated in Fig. 4 for $S_A^{(2)}$. In Fig. 4 (a) we show $S_A^{(2)}$ for $3 \leq W \leq 8$ as a function of U . A sharp change is visible at the phase transition. The data divided by W (Fig. 4 (b)) shows that in the Mott phase the entropy follows an area law and the behavior is fully reproduced by the perturbative result within the expected regime (continuous line). In the superfluid, $S_A^{(2)}$ shows strong finite size effects. In Fig. 4 (c), we show the contribution to $\text{Tr} \rho_A^2$ coming from the ES envelope (rhombi) and from the ES levels above (circles). The contribution of the non-envelope levels is much lower, especially in the superfluid (about four order of magnitude). This means that most of the contribution to $S_A^{(2)}$ comes from the envelope, which is responsible of the subleading logarithmic correction [6].

These results have implications for the range of applicability of DMRG calculations. The logarithmic contribution is due to the replication of the ES in every δN_A sector, which would be suppressed if δN_A was not a conserved quantity, as happens in DMRG calculations where the $U(1)$ symmetry is enforced to be broken. (See Refs. [21, 22] for analogous calculations in magnetic systems.) Our results thus provide a basis for a more quantitative explanation as to why explicitly symmetry-broken DMRG or MPS outperforms simulations exploiting the associated conserved quantum numbers in situations where continuous symmetry breaking takes place.

Discussion — We have presented a thorough analysis of the ES of the 2D Bose-Hubbard model, in particular highlighting very different structures of the ES in the Mott and superfluid phases. In the Mott phase, the ES can be understood perturbatively starting from the $U \rightarrow \infty$ product state limit. The ES is organized in a perturbative hierarchy and within each group there are dispersion structures reflecting the freedom of excitations to move along the boundary while retaining the same perturbation order. In the superfluid regime, the ES reflects the spontaneous symmetry breaking of the underlying state, and is related to the tower of states known from finite-size studies of physical spectra. We believe the major features addressed in the two phases are generic for a wide range of gapped and gapless 2D systems.

The results of the present work open up a number of open questions and research avenues. First, our analysis points to an advantage of DMRG calculations with enforced symmetry breaking; exploration of such techniques are yet to be attempted in detail. Second, it would be interesting to see the TOS structure appear for gapless phases where the symmetry breaking is more complex than the $U(1)$ symmetry broken in our case. The ES envelope would then be expected to have a nontrivial degeneracy structure, which would provide a more stringent demonstration of the correspondence between the ES and the TOS spectrum. Finally, the robust emergence of an area law in perturbation theory (cancellation of W^α terms with $\alpha > 1$) is not fully understood at this point, and deserves to be addressed in a more general setting.

We acknowledge stimulating discussions with T. Grover, M. Metlitski, and R.R.P. Singh. The DMRG simulations have been performed on machines of the platform "Scientific computing" at the University of Innsbruck - supported by the BMWF.

-
- [1] L. Amico, R. Fazio, A. Osterloh, and V. Vedral, *Rev. Mod. Phys.* **80**, 517 (2008).
 - [2] H. Li and F. D. M. Haldane, *Phys. Rev. Lett.* **101**, 010504 (2008). N. Regnault, B. A. Bernevig, F. D. M. Haldane, *Phys. Rev. Lett.* **103**, 016801 (2009). N. Bray-Ali, L. Ding, and S. Haas, *Phys. Rev. B* **80**, 180504(R) (2009). L. Fidkowski, *Phys. Rev. Lett.* **104**, 130502 (2010). A. M. Läuchli, E. J. Bergholtz, J. Suorsa, and M. Haque, *Phys. Rev. Lett.* **104**, 156404 (2010). R. Thomale, A. Sterdyniak, N. Regnault, and B. A. Bernevig, *Phys. Rev. Lett.* **104**, 180502 (2010). H. Yao and X. L. Qi, *Phys. Rev. Lett.* **105**, 080501 (2010). E. Prodan, T. L. Hughes, and B. A. Bernevig, *Phys. Rev. Lett.* **105**, 115501 (2010). F. Pollmann, A. M. Turner, E. Berg, M. Oshikawa, *Phys. Rev. B*, **81**, 064439 (2010). M. Kargarian and G. A. Fiete, *Phys. Rev. B*, **82**, 085106 (2010). A. M. Turner, Y. Zhang, A. Vishwanath, *Phys. Rev. B*, **82**, 241102R (2010). Z. Papic, B. A. Bernevig, and N. Regnault, *Phys. Rev. Lett.* **106**, 056801 (2011). L. Fidkowski, T. S. Jackson and I. Klich, *Phys. Rev. Lett.* **107**, 036601 (2011). J. Dubail, and N. Read, *Phys. Rev. Lett.* **107**, 157001 (2011). J. Schliemann, *Phys. Rev. B* **83**, 115322 (2011). T. L. Hughes, E. Prodan, B. A. Bernevig, *Phys. Rev. B*, **83**, 245132 (2011). N. Regnault and B. A. Bernevig, *Phys. Rev. X* **1**, 021014 (2011). X. L. Qi, H. Katsura, and A. W. W. Ludwig, *Phys. Rev. Lett.* **108**, 196402 (2012). D. Poilblanc, N. Schuch, D. Perez-Garcia, and J.I. Cirac, *Phys. Rev. B* **86**, 014404 (2012); N. Schuch, D. Poilblanc, J. I. Cirac, and D. Perez-Garcia, *arXiv:1210.5601* (unpublished).
 - [3] M. P. A. Fisher, P. B. Weichman, G. Grinstein, and D. S. Fisher, *Phys. Rev. B* **40**, 546 (1989).
 - [4] D. Jaksch, C. Bruder, J. I. Cirac, C. W. Gardiner, P. Zoller, *Phys. Rev. Lett.* **81** 3108 (1998).
 - [5] V. Alba, M. Haque and A. M. Läuchli, *Phys. Rev. Lett.* **108**, 227201 (2012).
 - [6] M. A. Metlitski and T. Grover, *arXiv:1112.5166*.
 - [7] C. Lhuillier, *arXiv:cond-mat/0502464v1* (unpublished).
 - [8] J. I. Cirac, D. Poilblanc, N. Schuch, and F. Verstraete, *Phys. Rev. B* **83**, 245134 (2011). I. Peschel and M.-C. Chung, *EPL* **96**, 50006 (2011).
 - [9] Additional detail is provided in the Supplementary Materials.
 - [10] B. Capogrosso-Sansone, S. G. Söyler, N. Prokof'ev, and B. Svistunov, *Phys. Rev. A* **77**, 015602 (2008).
 - [11] M. A. Metlitski and T. Grover, private communication.
 - [12] W. Ding and K. Yang, *Phys. Rev. A* **80**, 012329 (2009).
 - [13] V. Alba, M. Haque, and A. M. Läuchli; *J. Stat. Mech.* P08011 (2012). V. Popkov and M. Salerno, *Phys. Rev. A* **71**, 012301 (2005). M. Salerno and V. Popkov, *Phys. Rev. E* **82**, 011142 (2010). O. A. Castro-Alvaredo and B. Doyon, *J. Stat. Mech.* P02001 (2011).
 - [14] G. De Chiara, L. Lepori, M. Lewenstein, and A. Sanpera, *Phys. Rev. Lett.* **109**, 237208 (2012).
 - [15] A.J.A. James and R.M. Konik, *arXiv:1208.4033* (unpublished).
 - [16] M. S. L. du Croo de Jongh and J. M. J. van Leeuwen, *Phys. Rev. B* **57**, 8494 (1998).
 - [17] L. Tagliacozzo, G. Evenbly, and G. Vidal, *Phys. Rev. B* **80**, 235127 (2009).
 - [18] R. R. P. Singh, R. G. Melko, J. Oitmaa, *Phys. Rev. B* **86**, 075106 (2012).
 - [19] A. B. Kallin, M. B. Hastings, R. G. Melko, and R. R. P. Singh, *Phys. Rev. B* **84**, 165134 (2011).
 - [20] H. F. Song, N. Laflorencie, S. Rachel, and K. Le Hur, *Phys. Rev. B* **83**, 224410 (2011).
 - [21] S. R. White and A. L. Chernyshev, *Phys. Rev. Lett.* **99**, 127004 (2007).
 - [22] B. Bauer, P. Corboz, A.M. Läuchli, L. Messio, K. Penc, M. Troyer, and F. Mila, *Phys. Rev. B* **85**, 125116 (2012).

Supplementary Materials

OVERVIEW

In these Supplements, we provide additional details and information on several aspects of the ES of the 2D Bose-Hubbard model:

- We provide details on the perturbative expansions of the entanglement entropies in the Mott phase given in the paper. In particular we show that the expected area law behavior seems to be built into the structure of perturbation theory.
- We provide perturbative expressions in the Mott phase, up to the first few orders, for the entanglement Hamiltonian describing the levels of the ES envelope. We demonstrate that up to the first few orders the entanglement Hamiltonian has the form of a tight-binding 1D Hamiltonian for hard-core bosons, whose degrees of freedom are localized at the boundary between the two subsystems (boundary locality). By examining the sectors $\delta N_A = 1, 2$, we show that while in the Mott phase the entanglement Hamiltonian is short range it becomes long range as the Mott superfluid transition is approached.
- We discuss the $U = 0$ point. We show that the ES contains only one level in each sector δN_A for which we provide analytic expressions. The behaviors of the entanglement entropies and ‘gaps’ (Δ and δ) are discussed and compared with the interacting case $U \neq 0$.

ENTANGLEMENT ENTROPIES IN MOTT PHASE

As discussed in the main text, the entanglement entropies can be calculated perturbatively at large U . Here we provide expressions up to fourth order in $1/U$. This requires reduced density matrix eigenvalues λ_i (or ES levels ξ_i) up to order $\alpha = 2$ as defined in Figure 1 (left panel) of the main text.

We find that all the ES levels depend only on the boundary length W and not on the transverse size L , reflecting the boundary local nature of the ES. The perturbative expressions for ES levels contain terms nonlinear in W . Remarkably, at the orders we have calculated, these cancel when one constructs the Renyi and von Neumann entropies, giving rise to the expected area law ($\propto W$) behavior.

The reduced density matrix eigenvalues

We denote the eigenvalues of ρ_A at perturbative order α and particle number sector δN_A by $\lambda_i^{\{\alpha, \delta N_A\}}$, and the corresponding ES levels as $\xi_i^{\{\alpha, \delta N_A\}} = -\ln \lambda_i^{\{\alpha, \delta N_A\}}$. The index i labels the levels within each group at order α and sector δN_A .

$\alpha = 0$. Up to fourth order in $1/U$ the dominant eigenvalue (corresponding to the lowest ES level ξ_0) is given by

$$\lambda^{\{0,0\}} = 1 - 4W/U^2 - (488W - 8W^2)/U^4 + \mathcal{O}(U^{-5}) \quad (\text{S.1})$$

As may be expected from the boundary locality of the ES, the eigenvalue depends only on the boundary length W , and not on the cylinder length L in the direction transverse to the boundary. It is noteworthy that (S.1) contains terms nonlinear in W .

$\alpha = 1$. There are W levels at $\alpha = 1$ in the sector $\delta N_A = \pm 1$. Up to fourth order in $1/U$ we find

$$\lambda_j^{\{1, \pm 1\}} = \frac{2}{U^2} + \frac{148}{U^4} - W \frac{8}{U^4} + \frac{48}{U^3} \cos k_j + \frac{224}{U^4} \cos 2k_j + \mathcal{O}(U^{-5}) \quad (\text{S.2})$$

with $k_j \equiv 2\pi j/W$ ($j = 1, 2, \dots, W$).

$\alpha = 2$. Finally, we need to know the expansion of $\lambda^{\{2, \pm 2\}}$ and $\lambda^{\{2, 0\}}$. At $\alpha = 2$ order there are $W(W-1)/2$ eigenvalues each in sectors $\delta N_A = \pm 2$ and $W(W-1)$ in sector $\delta N_A = 0$ (Figure 1 of main article). All these eigenvalues are degenerate up to fourth order:

$$\lambda_i^{\{2, \pm 2\}} = \lambda_i^{\{2, 0\}} = \frac{4}{U^4} + \mathcal{O}(U^{-5}) \quad (\text{S.3})$$

Entanglement entropies

Using the perturbative results (S.1), (S.2), (S.3), we derive the corresponding expressions for the entropies.

The single copy entanglement. The single copy entanglement $S_A^{(\infty)}$ is obtained from (S.1) as

$$S_A^{(\infty)} = -\log \lambda^{\{0,0\}} \quad (\text{S.4})$$

which has the expansion

$$S_A^{(\infty)} = W \frac{4}{U^2} + W \frac{488}{U^4} + W^2 \frac{976}{U^6} - W^3 \frac{4}{U^6} + W^3 \frac{16}{3U^6} + \mathcal{O}(U^{-6}) \quad (\text{S.5})$$

Since (S.1) is correct only up to terms $\mathcal{O}(U^{-5})$, then in (S.5) only the terms up to fourth order are meaningful. It is remarkable that up to fourth order (S.5) contains only linear terms in W (area law), even though in (S.1) a quadratic term $\sim W^2$ is present. This term cancels when expanding the logarithm in (S.4). The $\sim U^{-6}$ terms apparently violate the area law but are not meaningful at this order and have to be discarded. At present we are unaware of any proof that higher powers of W must vanish at every perturbative order.

Renyi entropies. The expansion for the other Renyi entropies $S_A^{(\gamma)}$ ($\gamma \geq 2$) is obtained using

$$S_A^{(\gamma)} = -\frac{1}{n-1} \log \text{Tr} \rho_A^\gamma. \quad (\text{S.6})$$

For $\gamma = 2$ we have

$$\text{Tr} \rho_A^2 = 1 - W \frac{8}{U^2} - W \frac{968}{U^4} + W^2 \frac{32}{U^4} + \mathcal{O}(U^{-5}). \quad (\text{S.7})$$

Note again the presence of quadratic terms which arise from the multiplicity ($\sim W^2$) of $\lambda_i^{(2,\pm 2)}$ and $\lambda_i^{(2,0)}$. Plugging in (S.6) and expanding the logarithm we get

$$S_A^{(2)} = W \frac{8}{U^2} + W \frac{968}{U^4} + \mathcal{O}(U^{-5}). \quad (\text{S.8})$$

Again, we find the area law behavior up to meaningful order, due to the cancellation of W^2 terms as observed above for the single copy entanglement. Similar observations hold for the $\gamma = 3$ Renyi entropy:

$$\text{Tr} \rho_A^3 = 1 - W \frac{12}{U^2} - W \frac{2928}{U^4} + W^2 \frac{72}{U^4} + \mathcal{O}(U^{-5}). \quad (\text{S.9})$$

Von Neumann entropy. Up to order four the von Neumann entropy is

$$\begin{aligned} S_A &\equiv -\text{Tr} \rho_A \log \rho_A \\ &= -\lambda^{\{0,0\}} \log \lambda^{\{0,0\}} - \sum_{\delta \in \{-1,1\}} \sum_{i=1}^W \lambda_i^{\{1,\delta\}} \log \lambda_i^{\{1,\delta\}} \\ &\quad - \sum_{\delta \in \{-2,2\}} \sum_{i=1}^{W(W-1)/2} \lambda_i^{\{2,\delta\}} \log \lambda_i^{\{2,\delta\}} \\ &\quad - \sum_{i=1}^{W(W-1)} \lambda_i^{\{2,0\}} \log \lambda_i^{\{2,0\}} \end{aligned} \quad (\text{S.10})$$

Using (S.1), (S.2), (S.3), and the identity

$$\sum_{q=1}^W \cos(2\pi/Wrq) = W \delta_{r,0 \bmod W},$$

with r an integer, we obtain

$$S_A = 4W \left[\frac{1}{U^2} - \frac{1}{U^2} \log \frac{2}{U^2} - \frac{16}{U^4} \log \frac{2}{U^2} - \frac{146}{U^4} \right] + \mathcal{O}(U^{-5}). \quad (\text{S.11})$$

As observed for the Renyi entropies, although (S.1), (S.2), (S.3) contain non linear terms in W , the von Neumann entropy exhibits the area law behavior.

ENTANGLEMENT HAMILTONIAN FOR THE ES ENVELOPE

On the ES envelope in the Mott phase (Figure 1 of main article), at each nonzero δN_A there is a cluster of states which are described by an entanglement Hamiltonian and show corresponding dispersions. Below we give details for these entanglement Hamiltonians.

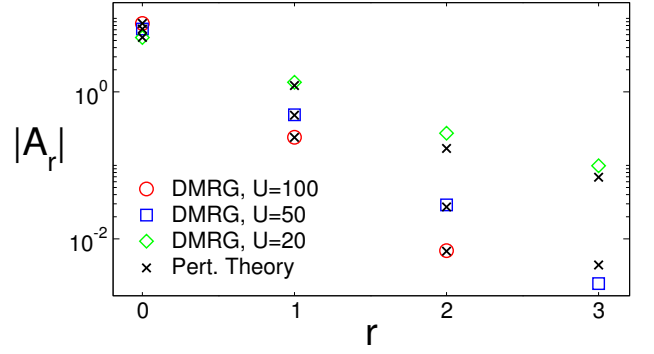


FIG. S1: Entanglement Hamiltonian for the envelope ES multiplet in the sector $\delta N_A = 1$. We plot the absolute value of the hopping amplitudes $|A_r|$ versus the hopping range r , on log-linear scale. The empty symbols are DMRG data in the Mott insulating phase (for a system of size $W = L/2 = 8$). Perturbation theory results are shown with crosses.

The $\delta N_A = 1$ sector. The entanglement Hamiltonian is given by the single particle hopping Hamiltonian

$$\mathcal{H}_E = \sum_{ir} A_r (a_i^\dagger a_{i+r} + h.c.) \quad (\text{S.12})$$

where $i = 1, 2, \dots, W$ labels the sites near the boundary between the two subsystems and $r = 0, 1, 2, \dots$ is the hopping range. Up to $\mathcal{O}(U^{-4})$ the hopping amplitudes are found to be

$$A_0 \equiv \log(U^2/2) + 2(2W + 10)/U^2 + \mathcal{O}(U^{-4}) \quad (\text{S.13})$$

$$A_1 \equiv -12 \left[1/U + (2W - 25)/(2U^3) \right] + \mathcal{O}(U^{-4})$$

$$A_2 \equiv -34/U^2 + \mathcal{O}(U^{-4})$$

$$A_3 \equiv 226/U^3 + \mathcal{O}(U^{-4})$$

In Fig. S1 we compare the theoretical predictions (S.13) with DMRG data. We consider a system of dimensions $W = L/2 = 8$ and $U = 20, 50, 100$. In Fig. S1 we show $|A_r|$ (for $r = 0, 1, 2, 3$) obtained from (S.13). We also plot the hopping amplitudes $|A_r|$ obtained by fitting the DMRG data to the single particle tight binding dispersion

$$\xi_m = A_0 + 2 \sum_{j=1}^3 A_j \cos \frac{2\pi}{W} m j. \quad (\text{S.14})$$

The perturbative expressions S.13 describe the DMRG data extremely well for $U = 50, 100$. Not surprisingly, the agreement is less perfect for $U = 20$ (the transition to the superfluid regime is at $U \approx 17$). The hopping amplitudes $|A_r|$ are seen to decay exponentially in the Mott phase with the hopping range r , but longer range hopping becomes more and more relevant as the superfluid transition is approached.

The $\delta N_A = 2$ sector. We provide the first two non zero orders (in $1/U$) for the entanglement Hamiltonian describing the levels of the ES envelope at $\delta N_A = 2$. The block in the reduced density matrix corresponding to this sector can

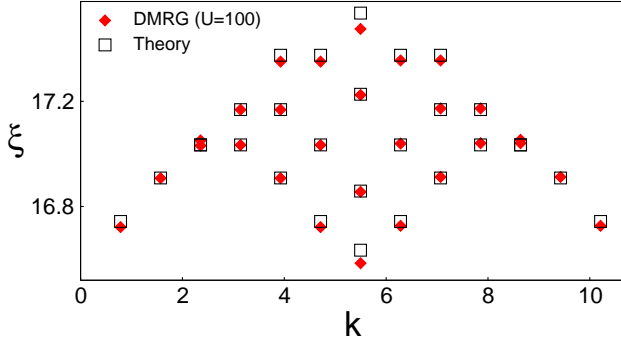


FIG. S2: Entanglement dispersion in the envelope ES levels at $\delta N_A = 2$. ES levels ξ are plotted against the momentum k along the boundary direction. Filled symbols are DMRG data at $U = 100$ for $W = L/2 = 8$. Empty symbols denote the theoretical prediction (S.18).

be written as

$$\rho_A(\delta N_A = 2) = \frac{4}{U^4} \sum_{i=1}^W \left[\frac{1}{2} a_i^\dagger a_i + \frac{12}{U} (a_i^\dagger a_{i+1} + h.c.) \right] + \dots \quad (\text{S.15})$$

where i labels the sites of subsystem A near the boundary, and a_i^\dagger are hard-core boson creation operators. The dots denote higher order corrections. The corresponding block in the entanglement Hamiltonian $\mathcal{H}_E \equiv -\log \rho_A$ is

$$\mathcal{H}_E(\delta N_A = 2) = 4 \log \frac{U}{\sqrt{2}} + \mathcal{H}' + \dots \quad (\text{S.16})$$

with

$$\mathcal{H}' \equiv -\frac{12}{U} \sum_{i=1}^W (a_i^\dagger a_{i+1} + h.c.). \quad (\text{S.17})$$

Apart from the constant shift $4 \log(U/\sqrt{2})$ the entanglement Hamiltonian is tight-binding Hamiltonian for two hard-core bosons, (S.17). Thus the ES levels in the envelope multiplet at $\delta N_A = 2$ can be obtained from the energy spectrum of two free hard-core bosons on a periodic chain. The single particle spectrum of (S.17) is given by

$$\epsilon_l = \begin{cases} -\frac{24}{U} \cos \frac{2\pi}{W} (l + \frac{1}{2}) & \text{if } W \text{ even} \\ -\frac{24}{U} \cos \frac{2\pi}{W} l & \text{if } W \text{ odd} \end{cases}$$

with $l = 0, 1, \dots, W-1$. The ES, i.e., the spectrum of (S.16), is obtained as

$$4 \log(U/\sqrt{2}) + \epsilon_{l_1} + \epsilon_{l_2} \quad (\text{S.18})$$

with $l_1 < l_2 = 0, 1, \dots, W-1$.

In Fig. S2 we show the ES levels in the envelope multiplet at $\delta N_A = 2$ (DMRG data for $U = 100$ and $W = L/2 = 8$). We also show the theoretical result (S.18) plotting the ES versus the momentum along the boundary $k = 2\pi l_1/W + 2\pi l_2/W$.

Since in our DMRG implementation we did not have access to the momentum, we assigned the momentum labels such that the data matches the theoretical prediction. (The procedure is not unique because ES levels with different momenta can be degenerate, but this is not important for present purposes.) Apart from small deviations due to higher order corrections in $1/U$, DMRG data are in agreement with (S.18).

The general case $\delta N_A > 2$. The result (S.18) can be extended to all the other clusters of levels in the ES envelope. The block in the entanglement Hamiltonian describing the envelope states at any δN_A is given (up to the first subleading order) by the tight-binding Hamiltonian for $|\delta N_A|$ hard-core bosons:

$$\mathcal{H}_E(\delta N_A) = 2|\delta N_A| \log \frac{U}{\sqrt{2}} + \mathcal{H}' + \dots \quad (\text{S.19})$$

with \mathcal{H}' given again by (S.17).

ES AT THE $U = 0$ POINT

Given a system of N non interacting bosons ($U = 0$), the ground state is an exact Bose condensate. All the bosons are in the single particle state

$$|\psi\rangle = \sum_{i=1}^V c_i b_i^\dagger |0\rangle \quad (\text{S.20})$$

with $V = LW$ the total number of sites of the system. (Since we consider unit filling we also have $N = V$.) Note that the “usual” Bose condensate in the state at zero momentum ($k = 0$) corresponds to the choice $c_i = \frac{1}{\sqrt{V}} \forall i$ in (S.20). This would give the correct ground state for non-interacting bosons on a torus. Since we are working on a cylindrical geometry this is not exactly correct in our case.

The ES obtained from the Bose condensate in the state (S.20) contains only one level in each sector with fixed N_A that is given by

$$\xi^{(N_A)} = -\log \left[\left(\sum_{i \in A} |c_i|^2 \right)^{N_A} \left(\sum_{i \in B} |c_i|^2 \right)^{N_B} \frac{N!}{N_A! N_B!} \right]. \quad (\text{S.21})$$

The ES (S.21) is continuously connected to the ES envelope upon switching on the interaction (at $U \neq 0$).

In other words, in the limit $U \rightarrow 0$ only the ES envelope survives and the higher parts of the ES are pushed to infinity. This implies that the gap Δ diverges ($\Delta \rightarrow \infty$) in the $U \rightarrow 0$ limit. In our DMRG data (Figure 3 bottom left in main article), we do not see a divergence for U as low as 2. This could be because the divergence starts at smaller U at these sizes, or that DMRG simulations with finite boson number cutoff per site is not able to capture this divergence.

For the toric geometry (when $c_i = 1/\sqrt{V}$) the ES (S.21) becomes

$$\xi^{(N_A)} = -\log \left[\frac{V_A^{N_A} V_B^{N_B}}{V^N} \right] + \log \left[\frac{N_A! N_B!}{N!} \right]. \quad (\text{S.22})$$

For our cylindrical geometry one obtains (S.22) only if block A is half of the system. Since this is the bipartition that we considered in the paper (and we expect that the physics remains unchanged for different bipartitions) we can use (S.22). Note that in the limit $\delta N_A \equiv N_A - N/2 \ll N$ the ES is exactly parabolic

$$\xi^{(N_A)} = -\frac{1}{2} \log \left(\frac{2}{V\pi} \right) + \frac{2}{V} (\delta N_A)^2. \quad (\text{S.23})$$

Strikingly, (S.23) implies $\delta \sim 1/V$, whereas at $U > 0$ the presence of sound waves (and of the ES levels above the envelope) implies $\delta \sim 1/W \sim 1/\sqrt{V}$ (as discussed in the

main text).

As a final remark, we mention that the entanglement entropy for non-interacting bosons does not obey the area law and in the limit $N \rightarrow \infty$ is given by

$$S_A \approx \frac{1}{2} \log N_A. \quad (\text{S.24})$$

This is consistent with the physics that the envelope in the gapless phase gives a logarithmic contribution to the entanglement entropies, while the area law is due to sound waves. Since sound waves are missing at $U = 0$, the coefficient of the area law term also vanishes in this limit.